

Biophysical homoeostasis of leaf temperature: a neglected process for vegetation and land-surface modelling

Article

Accepted Version

Dong, N., Prentice, I. C., Harrison, S. P. ORCID: <https://orcid.org/0000-0001-5687-1903>, Song, Q. H. and Zhang, Y. P. (2017) Biophysical homoeostasis of leaf temperature: a neglected process for vegetation and land-surface modelling. *Global Ecology and Biogeography*, 26 (9). pp. 998-1007. ISSN 1466-8238 doi: 10.1111/geb.12614 Available at <https://centaur.reading.ac.uk/72131/>

It is advisable to refer to the publisher's version if you intend to cite from the work. See [Guidance on citing](#).

To link to this article DOI: <http://dx.doi.org/10.1111/geb.12614>

Publisher: Wiley

All outputs in CentAUR are protected by Intellectual Property Rights law, including copyright law. Copyright and IPR is retained by the creators or other copyright holders. Terms and conditions for use of this material are defined in the [End User Agreement](#).

www.reading.ac.uk/centaur

CentAUR

Central Archive at the University of Reading

Reading's research outputs online

Biophysical homoeostasis of leaf temperature: a neglected process for vegetation and land-surface modelling

N. Dong^{1,3*}, I.C. Prentice^{1,2*}, S.P. Harrison^{1,3}, Q.H. Song⁴, Y.P. Zhang^{4,5}

¹Department of Biological Sciences, Macquarie University, North Ryde, NSW 2109, Australia

²AXA Chair Programme in Climate and Biosphere Impacts, Imperial College London, Department of Life Sciences, Silwood Park Campus, Buckhurst Road, Ascot, SL5 7PY, UK

³Centre for Past Climate Change and School of Archaeology, Geography and Environmental Sciences (SAGES), University of Reading, Whiteknights, RG6 6AH, Reading, UK

⁴Key Laboratory of Tropical Forest Ecology, Xishuangbanna Tropical Botanical Garden, Chinese Academy of Sciences, Menglun, 666303, China

⁵National Forest Ecosystem Research Station at Ailao Mountains, Jingdong 676200, China

*Joint first authors

Key words: leaf temperature, energy balance, crossover temperature, stomatal conductance, boundary-layer conductance, transpiration, DGVM, land-surface model

Corresponding author: ning.dong@students.mq.edu.au

The running title: Biophysical homoeostasis of leaf temperature

The number of references: 50 references

The number of words in the abstract: 235

The number of words in the main body: 4562

25 **ABSTRACT**

26 **Aim** Leaf and air temperatures are seldom equal, but many vegetation models assume
27 that they are. Land-surface models calculate canopy temperatures, but how well they
28 do so is unknown. We encourage consideration of leaf- and canopy-to-air temperature
29 differences (ΔT) as a benchmark for land-surface modelling, and an important feature
30 of plant and ecosystem function.

31 **Location** Tropical SW China.

32 **Methods** We illustrate diurnal cycles of leaf- and canopy-air temperature difference
33 (ΔT) with field measurements in a tropical dry woodland, and continuous monitoring
34 data in a tropical seasonal forest. The Priestley-Taylor (PT) and Penman-Monteith
35 (PM) approaches to evapotranspiration are used to provide insights into the
36 interpretation and prediction of ΔT . Field measurements are also compared to
37 land-surface model results obtained with the Joint UK Land Environment Simulator
38 (JULES) set up for the conditions of the site.

39 **Results** ΔT followed a consistent diurnal cycle with negative values at night (due to
40 negative net radiation) becoming positive in the morning, reaching a plateau and
41 becoming negative again when air temperature exceeded a “crossover” in the 24–29°C
42 range. Daily time courses of ΔT could be approximated by either the PT or PM model,
43 but JULES tended to underestimate the magnitude of negative ΔT .

44 **Main conclusions** Leaves with adequate water supply are partially buffered against
45 air-temperature variations, through a passive biophysical mechanism. This is likely
46 important for optimal leaf function, and land-surface and vegetation models should
47 aim to reproduce it.

48 INTRODUCTION

49 It has long been known that the temperature of leaves can differ by several degrees
50 (Campbell & Norman, 1998), and sometimes even by more than 10 degrees (Lange, 1959;
51 Gates *et al.*, 1964), from that of the surrounding air. Net radiation at the leaf surface must
52 be balanced by the combined fluxes of sensible and latent heat. The former is
53 proportional to the product of the leaf-to-air temperature difference (ΔT) and the leaf
54 boundary-layer conductance to heat. The latter is proportional to transpiration, which in
55 turn is proportional to the product of the leaf-to-air vapour pressure deficit (that is, the
56 vapour pressure deficit evaluated at the temperature of the leaf) and the combined
57 boundary-layer and stomatal conductances to water. ΔT adjusts rapidly to maintain this
58 balance.

59 The influence of leaf size and morphology on the leaf energy balance (through their
60 effects on boundary-layer conductance), and the implications of ΔT for photosynthesis,
61 transpiration and optimal leaf form, were active research topics in the 1960s and 1970s
62 (Linacre, 1964; Gates, 1968; Parkhurst & Loucks, 1972; Taylor, 1975; Givnish & Vermeij,
63 1976; Smith, 1978; Zangerl, 1978; Upchurch & Mahan, 1988). But Dynamic Global
64 Vegetation Models (DGVMs), first developed in the 1990s (reviewed by Prentice &
65 Cowling, 2013), have generally disregarded the biophysical effects of leaf size and
66 morphology and simply assumed $\Delta T = 0$. Biophysical land-surface models – used in
67 climate and Earth System models, and coupled to DGVMs in some cases – compute a
68 surface energy balance, and use the predicted canopy temperatures to drive leaf-level
69 physiological processes. But to our knowledge there has been no attempt to evaluate
70 these model predictions, or to analyse the implications of the modelled leaf-to-air
71 temperature differences for plant and ecosystem function.

As observed more than half a century ago by Gates (1964) and Linacre (1964, 1967), and discussed in two recent articles (Michaletz *et al.*, 2015, 2016), there is abundant empirical evidence that under well-watered conditions in the daytime leaves are generally warmer than air at low air temperatures but cooler than air at higher air temperatures – a phenomenon that has been called “limited homoeothermy” (Mahan & Upchurch, 1988, Upchurch & Mahan, 1988, Michaletz *et al.*, 2015, 2016). We prefer the term “biophysical homoeostasis”, which avoids any implied analogy with the metabolically active process of homoeothermy in animals. Leaves are generally cooler than air during the night and the periods just before sunset and just after sunrise, when net radiation is negative – in other words, there is net loss of energy from the land surface. In the daytime, leaf temperatures can be maintained within a narrower range than air temperatures, varying around a “crossover” or “equivalence” temperature (where $\Delta T = 0$) that can vary according to environmental conditions, but which generally lies within the optimum range for photosynthesis (Michaletz *et al.*, 2016). Oxygen isotope evidence suggests that the effective photosynthetic operating temperature in forest canopies varies surprisingly little from the boreal zone to the subtropics (Helliker & Richter, 2008) and is only a few degrees greater even in the tropics (Song *et al.*, 2011), indicating that leaves are partially buffered against spatial and temporal variations in the temperature of the air.

This Concept Paper aims to increase awareness of the biophysical causes and ecological significance of leaf-temperature homoeostasis, and to point out the potential use of canopy temperature as a benchmark for the evaluation and improvement of terrestrial ecosystem and land-surface models. We illustrate the temperature crossover phenomenon using (a) sequential field measurements on leaves of different species during two consecutive sampling days at a tropical dry woodland site, and (b) continuous monitoring of the upper canopy of an intact tropical seasonal forest. The Joint UK Land Environment Simulator (JULES), which provides the land-surface component of the UK Met Office

98 Hadley Centre Earth System Model (Best *et al.*, 2011), was set up for the specific
99 environmental conditions and vegetation composition of the site and the results compared
100 with our field measurements.

101 **THEORY**

102 Variations in ΔT (K) on a time scale of minutes or longer (Schymanski *et al.*, 2013) are
103 closely to the steady-state energy balance (see e.g. Jones 2013, p. 225):

$$104 \quad R_n - c_p g_b \Delta T - \lambda E = 0 \quad (1)$$

105 where R_n is the net radiation at the leaf surface (W m^{-2}), c_p is the specific heat capacity of
106 air at constant pressure ($\text{J mol}^{-1} \text{K}^{-1}$), g_b is the leaf boundary-layer conductance to heat
107 ($\text{mol m}^{-2} \text{s}^{-1}$), λ is the latent heat of vaporization of water (J mol^{-1}) and E is the
108 transpiration rate ($\text{mol m}^{-2} \text{s}^{-1}$). This equation states that the leaf-level net radiation is
109 balanced by the sum of the sensible and latent heat fluxes – the sensible heat flux
110 depending on ΔT as well as on g_b , which is inversely related to the thickness of the leaf
111 boundary layer. Larger leaves generally have lower g_b , as indicated by the empirical
112 equation $g_b = 0.135 \sqrt{(u/d)} \text{ mol m}^{-2} \text{s}^{-1}$ (Campbell & Norman, 1998, p. 101) where u is the
113 wind speed (m s^{-1}) and d is the characteristic dimension of the leaf (m) – about 0.74 times
114 the maximum width of the leaf (Taylor, 1975).

115 It follows by re-arrangement of equation (1) that:

$$116 \quad \Delta T = (R_n - \lambda E) / (c_p g_b) \quad (2)$$

117 Thus leaves are warmer than air if $R_n > \lambda E$, and more so for large leaves and at low wind
118 speeds. This explains why leaves have to be small in order to avoid overheating when air
119 temperatures are high and water is in short supply (Gates, 1968; Parkhurst & Loucks,
120 1972). However, under well-watered conditions, it is possible that $R_n < \lambda E$ if the air

temperature is high enough – resulting in leaves cooler than air. This cooling, relative to air temperature, is also stronger in large leaves and at low wind speeds.

One way to predict the sign and magnitude of ΔT invokes the equation of Priestley & Taylor (1972) (henceforth PT), an approximate empirical formula for evapotranspiration – either from freely evaporating (wet) surfaces, or from vegetation that is well supplied with soil moisture. The PT equation is based on the observation that the latent heat flux (λE) is strongly determined by the available energy supply (R_n):

$$\lambda E = \alpha [s/(s + \gamma)] R_n \quad (3)$$

where s is the derivative of the Clausius-Clapyeron relationship between saturated vapour pressure and temperature (Pa K^{-1}), evaluated at the ambient air temperature; γ is the psychrometer constant (Pa K^{-1}), equal to $P c_p / \lambda$ where P is atmospheric pressure (Pa); and α is a dimensionless parameter, found empirically to take values typically in the range 1.1 to 1.4 and with a canonical value of 1.26 (see e.g. McAneney & Itier, 1996; Jones, 2013, p. 109).

By combining equations (2) and (3), we obtain:

$$\Delta T = R_n \{1 - \alpha [s/(s + \gamma)]\} / (c_p g_b) \quad (4)$$

The ratio $s/(s + \gamma)$ is steeply dependent on air temperature, being 0.40 at 0°C, 0.55 at 10°C, 0.68 at 20°C, 0.78 at 30°C and 0.85 at 40°C. Setting $\alpha = 1.26$, equation (4) implies that there should be a crossover temperature (the value at which $\Delta T = 0$, implying $\alpha = 1 + \gamma/s$) around 31°C (Li *et al.*, 2013).

The predicted crossover temperature is sensitive to the value of α , however, and this parameter varies with environmental conditions. A number of studies (see e.g. Idso *et al.*,

1981; Michaletz *et al.*, 2016) have indicated lower crossover temperatures, in the range 25 to 28°C, consistent with somewhat larger values of α than the canonical 1.26.

There is an extensive literature (e.g. De Bruin, 1983; McNaughton & Spriggs, 1986; Lhomme, 1997; Huntingford & Monteith, 1998; Raupach, 2000) devoted to explaining in terms of more fundamental physical processes why α might be expected to be a relatively conservative quantity. The PT equation is an expression of the large-scale average evapotranspiration rate. It has also been applied successfully in the modelling of transpiration by leaf canopies (e.g. Agam *et al.* 2010). At the leaf scale, however, different plant species may have different traits influencing energy and water exchanges – including leaf orientations influencing R_n (Chow 1994), and stomatal and boundary-layer conductances – so there is likely to be variation among leaves, both above and below the large-scale integrated rate.

A more detailed model for the leaf-level energy balance can be derived using the so-called Penman linearization, which also underpins the Penman-Monteith (henceforth PM) combination equation for transpiration (see e.g. Jones, 2013, pp. 104-105). The Penman linearization approximates the leaf-to-air vapour pressure deficit via the initial terms of a Taylor series:

$$D(T + \Delta T) \approx D(T) + s \Delta T \quad (5)$$

where $D(T) = e_s(T) - e_a$ (with $e_s(T)$ the saturated water vapour pressure at air temperature T and e_a the actual water vapour pressure) and $D(T + \Delta T)$ is the same quantity evaluated at the leaf temperature. Equation (5) is a good approximation provided $\Delta T \ll T$. Equation (2) combined with equation (5) leads to:

$$\Delta T = [R_n - \lambda g \bullet (D + s \Delta T)/P] / (c_p g_b) \quad (6)$$

where g_{\bullet} is the combined (in series) stomatal and boundary-layer conductance to water, $g_{\bullet} = g_s g_b / (g_s + g_b)$ (the small difference between the boundary-layer conductances to water and heat is neglected here). Division by P is required for consistency with the molar units used for λ , g_s and g_b . As ΔT appears on both sides of equation (6), it is necessary to re-arrange it in order to solve for ΔT :

$$\Delta T = (R_n - \lambda g_{\bullet} D/P) / [c_p (g_b + \varepsilon g_{\bullet})] \quad (7)$$

with $\varepsilon = s/\gamma$. Equation (7) is equivalent to formulae given by Monteith & Szeicz (1962), Linacre (1972), Paw U (1984) and others. Campbell & Norman (1998, pp. 224-229) used this formulation to show how various plausible combinations of air temperature and vapour pressure deficit can lead to negative daytime values of ΔT .

Additional insight can be obtained by further manipulation of equation (7). A crossover temperature T_x can be inferred from equation (7) as the air temperature for which $\Delta T = 0$, implying that $D(T_x)/P = R_n/\lambda g_{\bullet}$ or, equivalently, $e_s(T_x)/P = R_n/\lambda g_{\bullet} + e_a/P$. It is plausible that the ratio of R_n to g_{\bullet} might be relatively conservative during the daytime due to the covariation of both R_n and g_s with irradiance, leading to a relatively conservative value of T_x . (This covariance must break down at night however, or near to dawn and dusk, as R_n is then dominated by the long-wave component). The definition $\gamma = Pc_p/\lambda$ allows equation (7) to be re-written in a compact form, as follows:

$$\Delta T = -[e_s(T) - e_s(T_x)] / [\gamma (1 + \varepsilon + g_b/g_s)] \quad (8)$$

if a value T_x is assumed to exist and e_a is assumed constant. Constancy of e_a is a reasonable assumption for variations in D that may be expected due to rapid air temperature changes during a day, when e_a normally varies much less than e_s . Because $e_s(T)$ increases steeply with T , equation (8) indicates that ΔT will be negative for all $T > T_x$. The rate of change of ΔT with T , evaluated at the crossover temperature T_x , is:

$$\partial(\Delta T)/\partial T = -\varepsilon/(1 + \varepsilon + g_b/g_s) \quad (9)$$

where ε is evaluated at T_x . Note that the rate of decrease in ΔT following equation (9) depends only on T_x and the ratio of g_b to g_s . The variation of leaf temperature with respect to air temperature (evaluated around $T = T_x$) has a slope that is less than unity by the amount given in equation (9).

A number of simplifications have been made in the treatment above. Michaletz *et al.* (2016) noted that (a) R_n is not independent of ΔT , as we have implicitly assumed so far, because the long-wave radiation emitted by the leaf increases with the fourth power of the leaf temperature following the Stefan-Boltzmann law; and (b) the Penman linearization, appropriate for small ΔT , becomes less accurate the further the leaf temperature departs from the air temperature. Point (a) is described in textbooks and a standard approximation exists to correct for it (see e.g. Jones, 2013, p. 225), allowing the isothermal net radiation (the value of R_n when $\Delta T = 0$) to be used in place of the true R_n in a more precise formula that accounts for the first-order effect of ΔT on R_n . Point (b) is dealt with in Michaletz *et al.* (2016) by representing $e_s(T)$ as a nearly exact fourth-degree polynomial in T , which can be combined with the known temperature-dependence of R_n leading to a quartic equation in T , which can be solved analytically. The reader is referred to Michaletz *et al.* (2016) for details.

METHODS AND RESULTS

Field measurements

The selected field site was in a tropical dry woodland, Mandan, Yunnan province, SW China (23.69° N, 101.85° E, 758 m a.s.l), with mean annual temperature 21.8°C and mean annual precipitation 981 mm. Solar noon occurs at 13:00 local time. Measurements were made at two topographic locations within the site, on two consecutive sunny days

during the dry season (October 2013). The location measured on the second day had slightly denser vegetation, apparently due to run-on from surrounding slopes. However, similar results were obtained for both days/locations. The canopy at both locations is sparse, so most leaves receive high illumination and fully sunlit leaves were readily accessible for measurement. Three species were selected. All were canopy-dominant small trees or tall shrubs, having sclerophyllous, hypostomatous leaves with typical areas of 25 cm² (*Terminthia paniculata*), 1 cm² (*Pistacia weinmannifolia*) and 0.9 cm² (*Osteosperma schwerinae*). The smaller leaves of the two latter species were closely packed along the branches, suggesting that their smaller size may not be biophysically significant. Each day, the temperatures of three replicate top-canopy sunlit leaves of each species were measured at half-hourly intervals using a hand-held infrared thermometer (The Fluke 574, Everett, USA), pre-calibrated by the manufacturer, with emissivity set to 0.98. Air temperature was recorded with a mercury thermometer. The stated measurement uncertainty of the infrared thermometer is ± 0.75 K and that of the mercury thermometer is ± 0.1 K. The uncertainty of our estimates of ΔT is therefore small compared to the range of observed ΔT (−6.2 to +7.5 K).

A consistent diurnal time course was observed across the different species and sampling days/locations (Fig. 1). The data points in Fig. 1 have been smoothed using a quadratic curve to highlight the characteristic diurnal pattern. ΔT was negative (reflecting negative R_n) in the early morning, became positive during the morning, then peaked and began to decline before solar noon (while R_n continued to increase). ΔT became negative again when the air temperature exceeded a crossover value in the range 26 to 28°C. There were no significant differences in observed crossover temperatures either among species or between days/locations. The observed values suggest α somewhat larger than 1.26, but well within the theoretically predicted range (up to 1.391 according to Huntingford &

Monteith, 1998). A similar diurnal time course of ΔT has been observed in other studies and environments, for example by Yu *et al.* (2015) in a desert.

Monitoring

Canopy temperature is continuously monitored at the flux tower site located in an intact tropical seasonal forest at Xishuangbanna Tropical Botanical Garden, XTBG (21.93°N, 101.27°E, 570 m a.s.l.), Yunnan province, China, with mean annual temperature 21.7°C and mean annual precipitation 1492 mm. Solar noon occurs at 13:15. An infrared temperature sensor (Apogee Instruments Inc., Logan, UT) has been installed 3 m above the canopy. Air temperature is monitored using the HMP45C instrument (Vaisala, Helsinki, Finland). Data are logged half-hourly.

We show the data from the dry season (January) of 2013 (Fig. 2). The same general diurnal time course is seen at canopy level in the seasonal forest (Fig. 2) as we observed at leaf level in the dry forest (Fig. 1). The observed crossover temperature was near 24°C.

A test of JULES with field measurements

We ran JULES in a standard configuration for stand-alone operation (i.e. not coupled to a climate model) with non-limiting soil moisture prescribed in all soil layers. Driving data on wind speed, relative humidity, and long- and short-wave radiation components through the days of measurement were obtained from the flux tower at Yuanjiang, 2 km from the field site. Appropriate values were prescribed in JULES for vegetation cover broken down by plant functional types (47% broadleaf evergreen trees, 3% C₃ grasses, 25% C₄ grasses, 12.5% shrubs and 12.5% bare ground) and soil properties (15% sand, 50% silt and 35% clay) based on a field assessment.

Fig. 3 compares the JULES results to our field measurements. The model simulates negative ΔT after about 14:00 local time, but the measurements show an earlier onset of negative values. Measured ΔT approached -6 K for each day/location and all species (Figs 1, 3), but JULES' simulated ΔT never fell below -2 K during the daytime.

Establishing the precise reasons for this discrepancy would require a series of sensitivity experiments to be carried out. However, we note that JULES simulates a precipitous decline in stomatal conductance from about 10:00 local time (Fig. 3), which would restrict transpiration rates.

Comparisons using simple analytical models

We attempted to fit our field-observed leaf-to-air temperature differences using both the PT and PM approaches (Fig. 4) by non-linear regression using the '*nls*' function in R. We treated α and g_b as the parameters to be estimated in equation (4) (PT), and g_b and g_{\bullet} as the parameters to be estimated in equation (7) (PM). Note that these model fits are approximate. A full implementation of the PM approach would require time-varying g_s , which was not measured. The assumption of constant g_b in both PT and PM models is also a simplification, as wind speed variations are expected to influence g_b . The fitted parameter values are given in Table 1. Negative ΔT was correctly simulated by both approaches (Fig. 4), with approximately the right timing and magnitude. Fig. 4 also shows JULES results for comparison and highlights the tendency of JULES to underestimate negative ΔT during the hottest part of the day.

We fitted equations (4) and (7) in the same way to the canopy monitoring data, including half-hourly measurements for each day during January 2013. For the PT model, the estimated α was 1.32 ± 0.005 ($p < 0.001$), corresponding to a crossover temperature of 26.8°C . The fitted value for g_b in equation (4) was $0.68 \pm 0.03 \text{ mol m}^{-2} \text{ s}^{-1}$ ($p < 0.001$). In

comparison to monitored canopy temperature, the PT model yielded a highly significant slope of 0.67 with $R^2 = 79\%$ (Fig. 5). For the PM model, we estimated a somewhat larger value of g_b ($1.45 \pm 0.02 \text{ mol m}^{-2} \text{ s}^{-1}$, $p < 0.001$), and $g_{\bullet} = 0.51 \pm 0.007 \text{ mol m}^{-2} \text{ s}^{-1}$. The regression between model predictions and the canopy monitoring data was again highly significant, with slope 0.94 and $R^2 = 85\%$ (Fig 5).

We also fitted both models to the monitoring data for each day separately (Appendix S2). This yielded for the PT model a median α of 1.34 (lower and upper quartiles: 1.32, 1.36) corresponding to a median crossover temperature of 26.0 (24.9, 27.3) °C, and fitted values for g_b in equation (4) of 0.61 (0.48, 0.68) $\text{mol m}^{-2} \text{ s}^{-1}$. For the PM model, we again estimated values of g_b larger than for the PT model: 1.45 (1.26, 1.66) $\text{mol m}^{-2} \text{ s}^{-1}$, and values of g_{\bullet} of 0.57 (0.50, 0.64) $\text{mol m}^{-2} \text{ s}^{-1}$. Both models fitted the monitoring canopy temperature well on visual comparison (Figs 5 and S2). A general underestimation of the magnitude of ΔT during the night (Fig. S2) probably relates to our simplifying assumption of constant g_b , neglecting the fact that wind speeds are generally lower at night than in the day. Low wind speeds would lead to smaller g_b and, accordingly, larger differences between canopy and air temperatures.

DISCUSSION

The thermal homeostasis of sunlit leaves is a passive mechanism, dependent on ample water supply for transpiration, which has the effect of keeping leaf temperatures in a more limited range than air temperatures. We observed leaves to be cooler than air during the midday period, even during the dry season in a tropical dry woodland (Fig. 1), presumably thanks to deep roots allowing water to continue to be transpired at a sufficiently high rate. However, along a gradient of declining rainfall, transpirational cooling must become ineffective at some point; so that the leaves will again be warmer

than the air during the hottest time of day. Where this point occurs along rainfall gradients remains to be determined.

Leaf-temperature homeostasis has important practical implications under climate warming scenarios. For example, the study of urban street trees by Leuzinger *et al.* (2010) projected extremely high future leaf temperatures, in scenarios where D was held constant. However, D is the proximal driver of transpiration rate, and it is expected to increase nearly everywhere (see e.g. Sherwood & Fu, 2014) – leading to reduced, and ultimately negative, ΔT . As air temperatures rise, even in temperate regions, the transpirational cooling effect of green infrastructure may become increasingly important for the environment of cities. Increased transpiration rates due to high D should also help to protect natural ecosystems and crops, to some extent, against potential adverse effects of high temperature. In this perspective, high D is not necessarily a stress on plants. Provided sufficient water is available for transpiration, high evaporative demand provides a degree of leaf-temperature buffering against high air temperatures.

DGVMs could be modified to include leaf-to-air temperature differences with the help of the theory discussed above. One key phenomenon that they currently do not capture is the negative feedback (via transpiration) under well-watered conditions, which maintains leaf temperatures within a more restricted range than air temperatures. DGVMs lacking this feedback are likely to overestimate the direct impacts of warming on the gas exchange of leaves in well-watered vegetation – including irrigated crops (Siebert *et al.*, 2017), and deeply-rooted plants even in relatively dry environments, as well as in moist forests. On the other hand, drought (in the sense of insufficient precipitation to support moist soils) is a potential double menace to tropical moist forests (Schymanski *et al.*, 2013) as stomatal closure under water limitation is expected to reduce transpiration; eventually to the point where negative ΔT is no longer possible – potentially compounding the effects of

hydraulic failure (Rowland *et al.*, 2015) with photosynthetic inhibition and even overheating damage. Deleterious effects of high leaf temperature would be felt soonest by large leaves, because of their low boundary-layer conductance. How the effective boundary-layer conductance actually varies under field conditions as a function of leaf morphology and canopy architecture remains a topic for investigation, potentially opening a route to the incorporation of more realistic plant functional diversity in DGVMs.

Land-surface models like JULES, designed for climate-model coupling, already contain the necessary equations (including explicit simulation of convective boundary layer dynamics and thermodynamics) to simulate canopy temperature from physical principles. However, to do so reliably, such models requires good representations of leaf boundary-layer and stomatal conductances. In JULES, the irradiance absorbed by the canopy follows Beer's law with a fixed light extinction coefficient based on the "big leaf" approach (Clark *et al.*, 2011), thus not allowing for possible variation in leaf-angle distributions. Stomatal conductance is treated as a decreasing function of vapour pressure deficit, following the Jacobs (1994) equation (Cox *et al.*, 1998). Boundary layer conductance is implicit, and cannot be altered in the current configuration of JULES. Our example indicates that the simulation of leaf energy balance with JULES might be inaccurate. In particular, the modelled cooling of leaves at high air temperatures was weaker than observed. Fig. 3 also indicates that stomatal closure was predicted to occur early in the day, restricting transpiration to a perhaps unrealistic extent. The "optimal stomatal conductance" equation, independently derived (from different assumptions) by Medlyn *et al.* (2011) and Prentice *et al.* (2014), implies that transpiration *continuously increases* with vapour pressure deficit despite partial stomatal closure; whereas the Jacobs equation used in JULES reduces g_s to a minimum value at a fixed maximum vapour pressure deficit. This difference may be important. Alternatively, or additionally,

reductions of transpiration at high temperatures – in the field (Duursma *et al.*, 2008, Medlyn *et al.* 2001), and in models like JULES that explicitly couple photosynthesis and stomatal behaviour – may be caused by the exceedance of photosynthetic temperature optima, prompting examination of whether the locations of these optima in current models (especially for tropical plant types) are realistic.

Leaf and canopy temperatures are measurable at spatial scales from field measurements on single leaves, through monitoring of vegetation canopies, to remotely sensed data at a global scale (Li *et al.*, 2015). As a sensitive indicator of the effectiveness of transpirational cooling, observations of ΔT would repay more extensive application to evaluate and improve the representation of vegetation-atmosphere energy and water exchanges in land-surface models, and plant functional diversity and climate-change impacts in DGVMs.

ACKNOWLEDGEMENTS

This research was supported by the Australian Research Council through a Discovery Grant ‘Next-generation vegetation modelling based on functional traits’ to ICP and Ian Wright. DN was supported by an international Macquarie Research Excellence Scholarship. We thank Martin Best, Jon Lloyd, Belinda Medlyn, Lina Mercado, Sean Michaletz, Anne Verhoef and Ian Wright for discussions; Lina Mercado and Felix Leung for JULES setup help; Jian Ni, Shuangxi Zhou, Yangyang Wu and Shubin Zhang for assistance in the field; and Stan Schymanski for detailed reviews of the manuscript. Fieldwork was funded by the State Key Laboratory of Environmental Geochemistry (SKLEG2013817) and the Hundred Talents Program of the Chinese Academy of Sciences (CAS) (2011031). Weather data were obtained from Yuanjiang Research Station for Savanna Ecosystems, Xishuangbanna Tropical Botanical Garden, Chinese Academy of Science. Monitoring was supported by the Joint National-Yunnan foundations ‘The

typical forest ecosystems response to climate change in Yunnan' (U1202234) and Yunnan Natural Science Foundation (2013FB077) grants to Y.P. Zhang. This work is a contribution to the AXA Chair Programme in Biosphere and Climate Impacts and the Imperial College initiative on Grand Challenges in Ecosystems and the Environment.

SUPPORTING INFORMATION

Appendix S1 Leaf temperature measurements and climate data at two topographic locations in a tropical dry woodland in Fig. 1(Mandan, Yunnan province, China).

Appendix S2 Diurnal cycles of observed (Fig. 5) canopy-to-air temperature differences compared with daily Priestley-Taylor (red) and Penman-Monteith (blue) simulations in a tropical seasonal forest (XTBG, Yunnan province, China).

Appendix S3 Parameters values in the Priestley-Taylor and Penman-Monteith models for the ΔT simulations in Fig S2, estimated from half-hourly canopy temperature monitoring.

DATA ACCESSIBILITY

Field data used in this study can be found in Appendix S1.

BIOSKETCH

ND's research aims for a better understanding of temperature effects on biological processes, and its application to large-scale vegetation models through a new approach that emphasizes simple, theoretical models to interpret observations on the interaction of traits and environment. ICP is a long-time pioneer of global vegetation modelling and is currently leading the development of a next-generation trait-based model for improved analysis of the coupling between biogeochemical and hydrological cycles, climate impacts and climate-vegetation feedbacks. SPH works on multiple aspects of global environmental and ecological data and their application to the modelling and

reconstruction of past environments. QHS works on ecosystem monitoring and analysis of forest canopy processes. YPZ leads research on global change and ecosystems at Xishuangbanna Tropical Botanical Garden.

REFERENCES

Agam, N., Kustas, W.P., Anderson, M.C., Norman, J.M., Colaizzi, P.D., Howell, T.A., Prueger, J.H., Meyers, T.P. & Wilson, T.B. (2010) Application of the Priestley–Taylor approach in a two-source surface energy balance model. *Journal of Hydrometeorology*, **11**, 185-198.

Best, M., Pryor, M., Clark, D., Rooney, G., Essery, R., Ménard, C., Edwards, J., Hendry, M., Porson, A. & Gedney, N. (2011) The Joint UK Land Environment Simulator (JULES), model description–Part 1: energy and water fluxes. *Geoscientific Model Development*, **4**, 677-699.

Campbell, G.S. & Norman, J.M. (1998) *An Introduction to Environmental Biophysics*, 2nd edn. Springer, New York.

Chow, W.S. (1994) Photoprotection and photoinhibitory damage. *Advances in Molecular and Cell Biology* (ed. by E.E. Bittar and J. Barber), pp. 151-196. Elsevier.

Clark, D., Mercado, L., Sitch, S., Jones, C., Gedney, N., Best, M., Pryor, M., Rooney, G., Essery, R. & Blyth, E. (2011) The Joint UK Land Environment Simulator (JULES), model description – Part 2: carbon fluxes and vegetation dynamics. *Geoscientific Model Development*, **4**, 701-722.

Cox, P., Huntingford, C. & Harding, R. (1998) A canopy conductance and photosynthesis model for use in a GCM land surface scheme. *Journal of Hydrology*, **212**, 79-94.

430 De Bruin, H.A.R. (1983) A model for the Priestley-Taylor parameter α . *Journal of*
431 *Climate and Applied Meteorology*, **22**: 572-578.

432 Duursma, R.A., Kolari, P., Perämäki, M., Nikinmaa, E., Hari, P., Delzon, S., Loustau, D.,
433 Ilvesniemi, H., Pumpanen, J. & Mäkelä, A. (2008) Predicting the decline in daily
434 maximum transpiration rate of two pine stands during drought based on constant
435 minimum leaf water potential and plant hydraulic conductance. *Tree Physiology*, **28**,
436 265-276.

437 Gates, D.M., Hiesey, W.M., Milner, H.W. & Nobs, M.A. (1964) Temperatures of *Mimulus*
438 leaves in natural environments and in a controlled chamber. *Carnegie Institution of*
439 *Washington Yearbook*, **63**, 418-426.

440 Gates, D.M. (1968) Transpiration and leaf temperature. *Annual Review of Plant*
441 *Physiology*, **19**, 211-238.

442 Givnish, T.J. & Vermeij, G.J. (1976) Sizes and shapes of liane leaves. *The American*
443 *Naturalist*, **110**, 743-778.

444 Helliker, B.R. & Richter, S.L. (2008) Subtropical to boreal convergence of tree-leaf
445 temperatures. *Nature*, **454**, 511-514.

446 Huntingford, C. & Monteith, J.L. The behaviour of a mixed-layer model of the
447 convective boundary layer coupled to a big leaf model of surface energy partitioning.
448 *Boundary-Layer Meteorology*, **88**, 87-101.

449 Idso, S.B., Reginato, R.J., Jackson, R.D. & Pinter, P.J. (1981) Foliage and air
450 temperatures: Evidence for a dynamic “equivalence point”. *Agricultural Meteorology*, **24**,
451 223-226.

452 Jacobs, C. (1994) Direct impact of atmospheric CO₂ enrichment on regional transpiration.
 453 PhD thesis, Wageningen Agricultural University.

454 Jones, H.G. (2013) *Plants and Microclimate: a quantitative Approach to Environmental*
 455 *Plant Physiology*, 3rd edn. Cambridge University Press, Cambridge.

456 Lange O.L. (1959) Untersuchungen über Wärmehaushalt und Hitzeresistenz
 457 mauretanischer Wüsten- und Savannenpflanzen. *Flora*, **147**, 595-651.

458 Leuzinger, S., Vogt, R. & Körner, C. (2010) Tree surface temperature in an urban
 459 environment. *Agricultural and Forest Meteorology*, **150**, 56-62.

460 Lhomme, J.P. (1997) An examination of the Priestley-Taylor equation using a convective
 461 boundary layer model. *Water Resources Research*, **33**, 2571-2578.

462 Li, G., Harrison, S.P., Bartlein, P.J., Izumi, K. & Prentice, I.C. (2013) Precipitation
 463 scaling with temperature in warm and cold climates: an analysis of CMIP5 simulations.
 464 *Geophysical Research Letters*, **40**, 4018-4024.

465 Li, Y., Zhao, M., Motesharrei, S., Mu, Q., Kalnay, E. & Li, S. (2015) Local cooling and
 466 warming effects of forests based on satellite observations. *Nature Communication*, **6**.

467 Linacre, E. (1964) A note on a feature of leaf and air temperatures. *Agricultural*
 468 *Meteorology*, **1**, 66-72.

469 Linacre, E. (1967) Further studies of the heat transfer from a leaf. *Plant physiology*, **42**,
 470 651-658.

471 Linacre, E. (1972) Leaf temperatures, diffusion resistances, and transpiration.
 472 *Agricultural Meteorology*, **10**, 365-382.

473 Mahan, J.R. & Upchurch, D.R. (1988) Maintenance of constant leaf temperature by
 474 plants I. Hypothesis – limited homeothermy. *Environmental and Experimental Botany*, **28**,
 475 351-357.

476 McAneney, K.J. & Itier, B. (1996) Operational limits to the Priestley-Taylor formula.
 477 *Irrigation Science*, **17**, 37-43.

478 McNaughton, K., & Spriggs, T.(1986) A mixed-layer model for regional evaporation.
 479 *Boundary-layer Meteorology*, **34**, 243-262.

480 Medlyn, B.E., Barton, C.V.M., Broadmeadow, M.S.J., Ceulemans, R., De Angelis, P.,
 481 Forstreuter, M., Freeman, M., Jackson, S.B., Kellomäki, S., Laitat, E., Rey, A., Roberntz,
 482 P., Sigurdsson, B.D., Strassemeier, J., Wang, K., Curtis, P.S. & Jarvis, P.G. (2001)
 483 Stomatal conductance of forest species after long-term exposure to elevated CO₂
 484 concentration: a synthesis. *New Phytologist*, **149**, 247-264.

485 Medlyn, B.E., Duursma, R.A., Eamus, D., Ellsworth, D.S., Prentice, I.C., Barton, C.V.M.,
 486 Crous, K.Y., De Angelis, P., Freeman, M. & Wingate, L. (2011) Reconciling the optimal
 487 and empirical approaches to modelling stomatal conductance. *Global Change Biology*, **17**,
 488 2134-2144.

489 Mercado, L.M., Huntingford, C., Gash, J.H.C., Cox, P.M. & Jogireddy, V. (2007)
 490 Improving the representation of radiation interception and photosynthesis for climate
 491 model applications. *Tellus B*, **59**, 553-565.

492 Michaletz, S.T., Weiser, M.D., Zhou, J., Kaspari, M., Helliker, B.R. & Enquist, B.J. (2015)
 493 Plant thermoregulation: energetics, trait-environment interactions, and carbon economics.
 494 *Trends in Ecology and Evolution*, **30**, 714-724.

495 Michaletz, S.T., Weiser, M.D., McDowell, N.G., Zhou, J., Kaspari, M., Helliker, B.R. &
 496 Enquist, B.J. (2016) The energetic and carbon economic origins of leaf thermoregulation.
 497 *Nature Plants*, **2**, 16129.

498 Monteith, J.L. & Szeicz, G. (1962) Radiative temperature in the heat balance of natural
 499 surfaces. *Quarterly Journal of the Royal Meteorological Society*, **88**, 496-507.

500 Monteith, J.L. (1995) A reinterpretation of stomatal responses to humidity. *Plant, Cell &*
 501 *Environment*, **18**, 357-364.

502 Parkhurst, D.F. & Loucks, O. (1972) Optimal leaf size in relation to environment.
 503 *Journal of Ecology*, **60**, 505-537.

504 Paw U, K.T. (1984) A theoretical basis for the leaf equivalence point temperature.
 505 *Agricultural meteorology*, **30**, 247-256.

506 Prentice, I.C. & Cowling, S.A. (2013) Dynamic global vegetation models. *Encyclopedia*
 507 *of Biodiversity*, **2**, 607-689.

508 Prentice, I.C., Dong, N., Gleason, S.M., Maire, V. & Wright, I.J. (2014) Balancing the
 509 costs of carbon gain and water transport: testing a new theoretical framework for plant
 510 functional ecology. *Ecology Letters*, **17**, 82-91.

511 Priestley, C. & Taylor, R. (1972) On the assessment of surface heat flux and evaporation
 512 using large-scale parameters. *Monthly Weather Review*, **100**, 81-92.

513 Raupach, M. (2000) Equilibrium evaporation and the convective boundary layer.
 514 *Boundary-layer Meteorology*, **96**, 107-142.

515 Rowland, L., da Costa, A.C.L., Galbraith, D.R., Oliveira, R.S., Binks, O.J., Oliveira,
 516 A.A.R., Pullen, A.M., Doughty, C.E., Netcalfe, D.B., Vasconcelos, S.S., Ferreira, L.V.,

517 Malhi, Y., Grace, J., Mencuccini, M. & Meir, P. (2015) Death from drought in tropical
518 forests is triggered by hydraulics not carbon starvation. *Nature*, **528**, 119-122.

519 Schymanski, S.J., Or, D. & Zwieniecki, M. (2013) Stomatal control and leaf thermal and
520 hydraulic capacitances under rapid environmental fluctuations. *PLOS One*, **8**, e54231.

521 Siebert, S., Webber, H., Zhao, G. & Ewert, F. (2017) Heat stress is overestimated in
522 climate impact studies for irrigated agriculture. *Environmental Research Letters*, **12**,
523 054023.

524 Sherwood, S. & Fu, Q. (2014) A drier future? *Science* **343**, 737-739.

525 Smith, W.K. (1978) Temperatures of desert plants: another perspective on the adaptability
526 of leaf size. *Science*, **201**, 614-616.

527 Song, X., Barbour, M.M., Saurer, M., Helliker, B.R. (2011) Examining the large scale
528 convergence of photosynthesis weighted tree leaf temperatures through stable oxygen
529 isotope analysis of multiple data sets. *New Phytologist*, **192**, 912-924.

530 Taylor, S.E. (1975) Optimal leaf form. *Perspectives of Biophysical Ecology* (ed. by D.M.
531 Gates & R.B. Schmerl), pp. 73-86. Springer, Berlin, Heidelberg.

532 Upchurch, D.R. & Mahan, J.R. (1988) Maintenance of constant leaf temperature by
533 plants II. Experimental observations in cotton. *Environmental and Experimental Botany*,
534 **28**, 359-366.

535 Yu, M.-H., Ding, G.-D., Gao, G.-L., Sun, B.-P., Zhao, Y.-Y., Wan, L., Wang, D.-Y. & Gui,
536 Z.-Y. (2015) How the plant temperature links to the air temperature in the desert plant
537 *Artemisia ordosica*. *PLOS One*, **10**, e0135452.

538 Zangerl, A.R.(1978) Energy exchange phenomena, physiological rates and leaf size
539 variation. *Oecologia*, **34**, 107-112.

Table 1. Parameter values (with standard errors) and goodness-of-fit statistics in the Priestley-Taylor and Penman-Monteith models for leaf-to-air temperature difference (ΔT , K) as given in Fig 4, estimated from field measurements during the second day in a tropical dry woodland site (Mandan, Yunnan province, China).

<i>Priestley-Taylor model</i>			
	<i>T. paniculata</i>	<i>P. weinmannifolia</i>	<i>O. schwerinae</i>
α (–)	1.27 ± 0.03	1.31 ± 0.01	1.32 ± 0.01
g_b (mol m ⁻² s ⁻¹)	0.52 ± 0.25	0.20 ± 0.03	0.24 ± 0.04
RMSE (K)	1.97	1.63	1.31
<i>Penman-Monteith model</i>			
	<i>T. paniculata</i>	<i>P. weinmannifolia</i>	<i>O. schwerinae</i>
g_b (mol m ⁻² s ⁻¹)	1.07 ± 0.35	0.86 ± 0.38	1.17 ± 0.55
g_{\bullet} (mol m ⁻² s ⁻¹)	0.53 ± 0.07	0.67 ± 0.1	0.73 ± 0.12
RMSE (K)	1.97	1.63	1.31

546 **FIGURE CAPTIONS**

547 **Figure 1** Diurnal time courses of the leaf-to-air temperature difference (ΔT , K) during the
548 dry season (October 2013) for three species, measured on consecutive days at two
549 topographic locations in a tropical dry woodland site (Mandan, Yunnan province, China).
550 The top panel displays measurements from the first day and the bottom panel from the
551 second day. Species: *Terminthia paniculata*, *Pistacia weinmannifolia*, *Osteosperma*
552 *schwerinae*. Vertical bars are standard errors of three replicates. Fitted smooth curves are
553 quadratic regressions against time (solid) with 95% confidence intervals (dashed). The
554 left-hand panels show measured half-hourly net radiation (R_n , W m^{-2}) from the nearest
555 meteorological station (Yuanjiang) during sampling, and field-measured ambient
556 temperatures (T_{air} , $^{\circ}\text{C}$). Vertical dashed lines mark solar noon. Horizontal dashed lines
557 mark $\Delta T = 0$.

558 **Figure 2** Diurnal time courses of the canopy-to-air temperature difference (ΔT , K) and
559 canopy temperature during the dry season (January 2013) in a continuous tropical
560 seasonal forest (Xishuangbanna Tropical Botanical Garden, Yunnan province, China).
561 Vertical bars are standard errors across the 31 days. Vertical dashed lines mark solar noon.
562 Shaded areas represent the daylight period.

563 **Figure 3** (a) Diurnal time courses of JULES-simulated canopy temperature and observed
564 leaf temperatures during the sampling days shown in Fig. 1. (d-f). Different coloured
565 symbols represent observed leaf temperatures of the three species. Air temperatures and
566 simulated soil temperatures are also shown. (b) Diurnal time courses of stomatal
567 conductance from JULES. Shaded areas represent the sampling period. Vertical dashed
568 lines mark solar noon.

569 **Figure 4** Diurnal time courses of (a) net radiation (R_n , W m^{-2}) and ambient temperature
570 (T_{air} , $^{\circ}\text{C}$), (b) vapour pressure deficit (D , in kPa) and (c) actual vapour pressure (e_a , kPa)
571 at Yuanjiang meteorological station during the sampling days shown in Fig. 1. (d-f)

Diurnal time courses of observed leaf-to-air temperature differences (ΔT , K) for the three species, compared to modelled values obtained with the Priestley-Taylor and Penman-Monteith approaches, and with the JULES land-surface model. Green circles are observed leaf temperatures of the three species. Vertical dashed lines mark solar noon. Shaded area represents the daylight period.

Figure 5 The Priestley-Taylor and Penman-Monteith simulations for ΔT fitted to half-hourly canopy-to-air temperature differences obtained from continuous monitoring in a tropical seasonal forest (Xishuangbanna Tropical Botanical Garden, Yunnan province, China) during the dry season (January 2013).

FIGURES

Figure 1

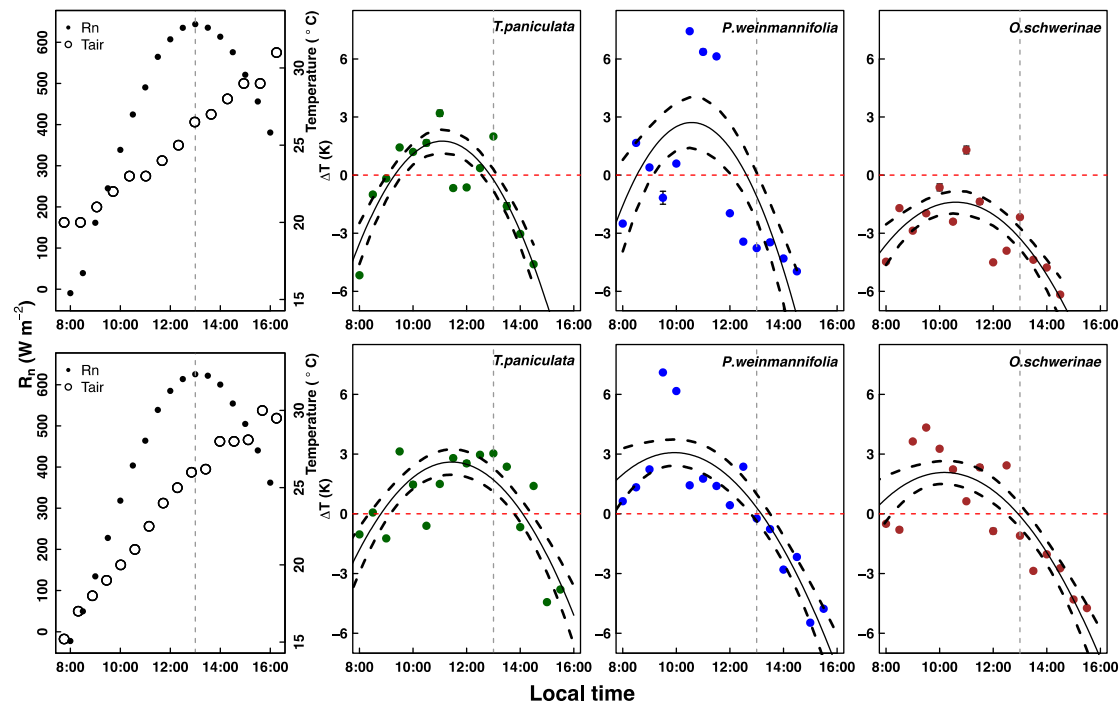
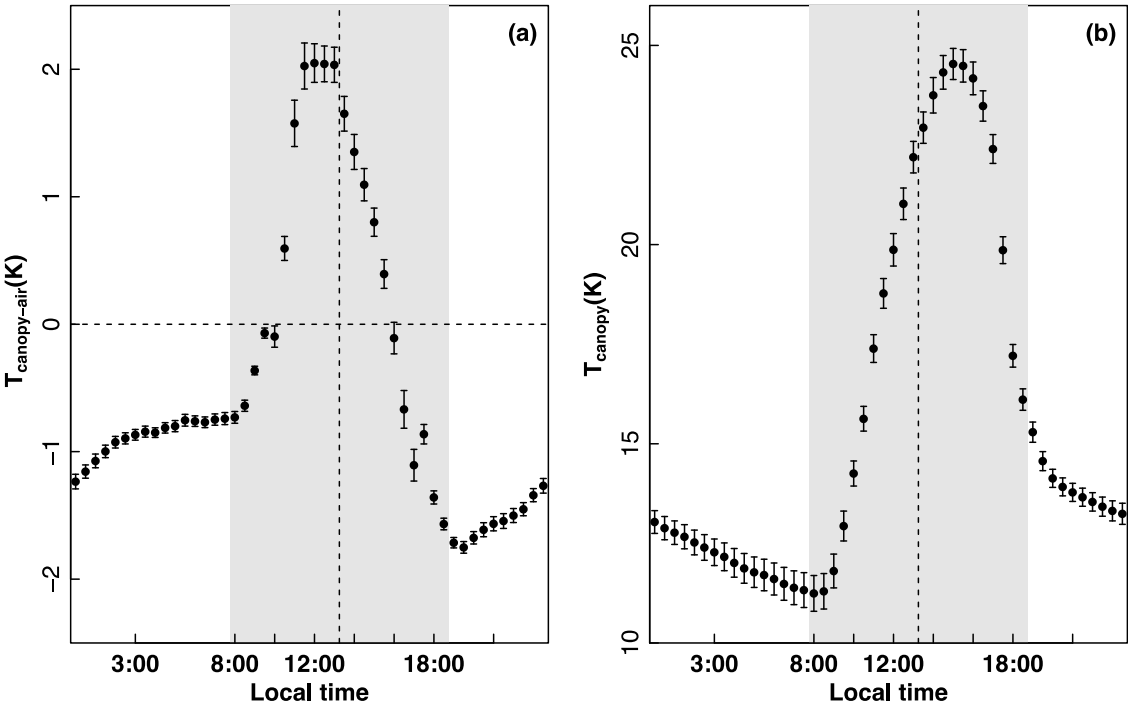
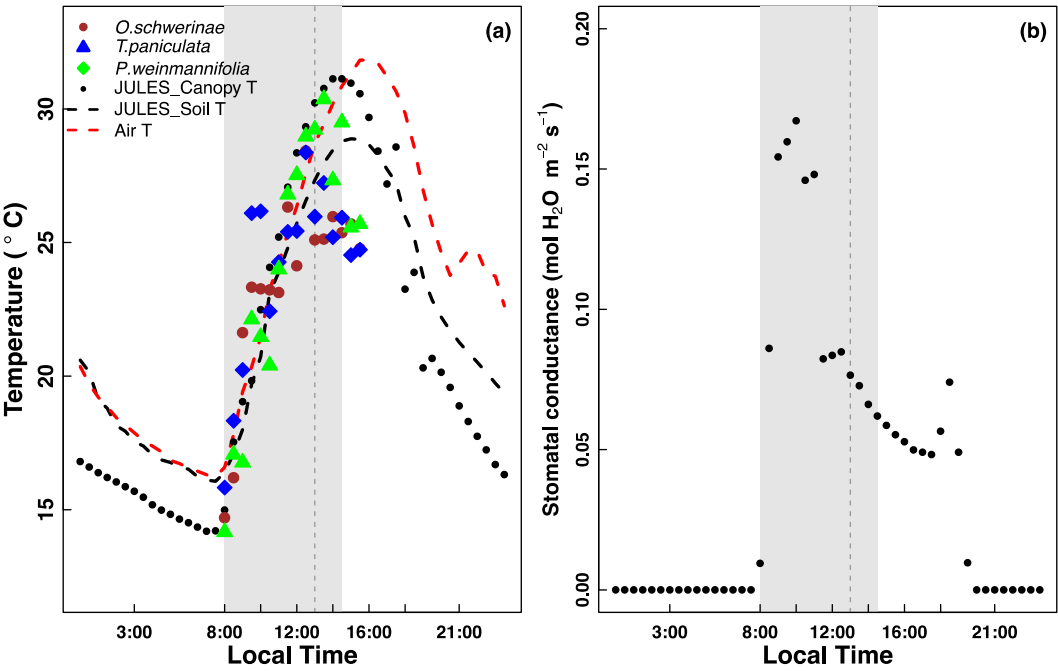


Figure 2



590 **Figure 3**



591

592

Figure 4

